

# Computational modeling of cardiovascular response to orthostatic stress

THOMAS HELDT,<sup>1</sup> EUN B. SHIM,<sup>2</sup> ROGER D. KAMM,<sup>3</sup> AND ROGER G. MARK<sup>1</sup>

<sup>1</sup>*Harvard University-Massachusetts Institute of Technology Division of Health Sciences and Technology, Massachusetts Institute of Technology, Cambridge, Massachusetts;*

<sup>2</sup>*Kumoh National University of Technology, Kumi, Kyungbuk, 730-701, Republic of Korea;*

<sup>3</sup>*Division of Bioengineering and Environmental Health, Massachusetts Institute of Technology, Cambridge, Massachusetts 02139*

Received 13 March 2001; accepted in final form 19 November 2001

**Heldt, Thomas, Eun B. Shim, Roger D. Kamm, and Roger G. Mark.** Computational modeling of cardiovascular response to orthostatic stress. *J Appl Physiol* 92: 1239–1254, 2002; 10.1152/jappphysiol.00241.2001.—The objective of this study is to develop a model of the cardiovascular system capable of simulating the short-term ( $\leq 5$  min) transient and steady-state hemodynamic responses to head-up tilt and lower body negative pressure. The model consists of a closed-loop lumped-parameter representation of the circulation connected to set-point models of the arterial and cardiopulmonary baroreflexes. Model parameters are largely based on literature values. Model verification was performed by comparing the simulation output under baseline conditions and at different levels of orthostatic stress to sets of population-averaged hemodynamic data reported in the literature. On the basis of experimental evidence, we adjusted some model parameters to simulate experimental data. Orthostatic stress simulations are not statistically different from experimental data (two-sided test of significance with Bonferroni adjustment for multiple comparisons). Transient response characteristics of heart rate to tilt also compare well with reported data. A case study is presented on how the model is intended to be used in the future to investigate the effects of postspaceflight orthostatic intolerance.

mathematical model; simulation; head-up tilt; lower body negative pressure; orthostatic intolerance

A MAJOR CARDIOVASCULAR PROBLEM in the present life-science space program is orthostatic intolerance (OI) seen in astronauts on their return to the normal gravitational environment (16). Many hypotheses concerning the mechanisms leading to OI have been the focus of in-flight and ground-based experimental studies in the past, and some are presently under investigation in both human and animal studies (see Table 1). Despite considerable efforts, there remains a lack of universal consensus about the fundamental etiology of postflight OI. To quantitatively supplement some of these studies, we have developed a computational model capable of simulating the short-term ( $\leq 5$  min) response of the

cardiovascular system to gravitational challenge in normal and microgravity-adapted individuals.

The response of the cardiovascular system to both orthostatic stress and the microgravity environment has been the focus of several mathematical models in the past (11, 18, 42, 50, 51, 78, 79). Modeling efforts ranged from explaining observations seen during spaceflight (78) to simulating the physiological response of ground-based experiments such as lower body negative pressure (LBNP) and head-up tilt (HUT) (11, 18, 42, 50, 51, 72, 80). Investigations of potential countermeasures to the adverse effects of re-entry into the Earth's gravitational environment after exposure to weightlessness have also been supplemented by computer models (64, 65, 71). Melchior et al. (49) analyzed a number of the models previously used and summarized some of the general requirements thought to be important in simulating the short-term response to orthostatic stress.

Several mathematical models dedicated particularly to simulating the systems-level response of the cardiovascular system to orthostatic stress have appeared in the literature over the past three decades (11, 18, 42, 50, 51, 72). In an early effort to simulate the hemodynamic response to changes in posture, Boyers and co-workers (11) implemented a seven-compartment steady-state model of the cardiovascular system connected to models of the arterial baroreflex and the cardiopulmonary baroreflex. In a later study, Croston and Fitzjerrell (18) devised a 28-compartment lumped-parameter model that is very similar in design to the one presented in this paper: arterial, venous, and cardiac compartments are modeled in terms of coupled ordinary differential equations that describe the dynamics of the system. Their control model representation is very elaborate, with total metabolites and oxygen debt being input parameters in addition to arterial pressure. Melchior and co-workers (50) simulated the hemodynamic response to LBNP by employing a four-

Address for reprint requests and other correspondence: R. G. Mark, Massachusetts Institute of Technology, Rm. E25-505, 77 Massachusetts Ave., Cambridge, MA 02139.

The costs of publication of this article were defrayed in part by the payment of page charges. The article must therefore be hereby marked "advertisement" in accordance with 18 U.S.C. Section 1734 solely to indicate this fact.

Table 1. *Mechanisms thought to contribute to postspaceflight orthostatic intolerance*

Mechanism	Reference
Hemodynamic mechanisms	
Hypovolemia	40, 41
Decreased venous capacitance	15, 74
Cardiac atrophy	8, 29, 43
Reflex mechanisms	
Central dysfunction	26
End-organ dysfunction	14, 17
Noncardiovascular mechanisms	
Neurovestibular dysfunction	82
Musculoskeletal causes	15
Aerobic fitness	44

step open-loop steady-state model in which changes in venous blood distribution affect mean arterial pressure, stroke volume, heart rate, and peripheral resistance. In a subsequent extension of their work (51), the authors refined their modeling strategy by including a pelvic venous compartment and a Windkessel model of the systemic circulation. Sud and co-workers (72) devised an elaborate finite-element model of the uncontrolled circulation to investigate the effects of LBNP on regional blood flow.

The primary objective of the work presented in this paper is to develop and test a general modular model of cardiovascular function that contains the essential features associated with the effects of gravity. In particular, we present a single cardiovascular model capable of simulating the steady-state and transient response to two orthostatic stress tests, namely HUT and LBNP, and compare the simulations to population-averaged hemodynamic data.

By implementing HUT and LBNP interventions and comparing the simulation results to experimental observations of the general population, we validate our simulations against a larger pool of experimental studies than was possible in previous modeling studies. In a case study, we show how the model may be used to demonstrate the impact of changes in individual parameters on the heart rate dynamics during orthostatic stress. By comparing these simulations to individual subject data from astronauts before and after exposure to microgravity, we can evaluate whether or not a particular hypothesis regarding the mechanisms underlying postspaceflight OI can account for the change seen in the data. The model thus provides a framework with which to interpret experimental observations and to evaluate alternative physiological hypotheses of the cause of OI.

Despite the fact that we tried as much as possible to give a detailed account of the origin of the parameter values, we acknowledge that uncertainties in the parameter assignments continue to persist.

Much like previously reported models (21, 79), our model is based on a closed-loop lumped-parameter hemodynamic model with regional blood flow to major peripheral circulatory branches. Features such as nonlinear regional venous compliances and venous valves

have been implemented in accordance with previous work (79). Dynamic change in intravascular volume during orthostatic stress is, however, an added feature of our model that has not previously been implemented for short-term studies and is of critical importance in simulating tilt and LBNP maneuvers (49). Blood pressure homeostasis is maintained in our model with the aid of the two major neural reflex control loops: the arterial baroreflex and the cardiopulmonary reflex. Unlike earlier models (18, 50, 51, 79), we emphasize the separation of sympathetic and parasympathetic reflex limbs. Furthermore, the four effector mechanisms (heart rate, cardiac contractility, regional peripheral resistance, and regional venous tone) have gain values that can be specified independently. Because autonomic dysfunction is believed to be at least in part responsible for OI (53), the ability to modify the control of the heart and various vascular beds independently makes this model a powerful tool to investigate present hypotheses concerning the mechanisms underlying OI.

## THE HEMODYNAMIC MODEL

### Architecture

We have extended a previously published (21) closed-loop lumped-parameter model of the cardiovascular system to facilitate anatomically specific representation of gravitational and LBNP stresses and of regionally specific cardiovascular compensatory mechanisms.

The hemodynamic model is mathematically formulated in terms of an electric analog model in which inertial effects are neglected. All resistors and most capacitors are assumed to be linear. These model assumptions lead to governing differential equations that are of first order. Figure 1 shows the  $n$ th compartment.

The flow rates ( $q$ ) across the resistors ( $R$ ) and capacitor ( $C$ ) expressed in terms of the pressures ( $P$ ) are given by

$$q_1 = (P_{n-1} - P_n)/R_n$$

$$q_2 = (P_n - P_{n+1})/R_{n+1}$$

$$q_3 = d/dt[C_n \times (P_n - P_{bias})]$$

See Fig. 1 legend for definition of subscripts.

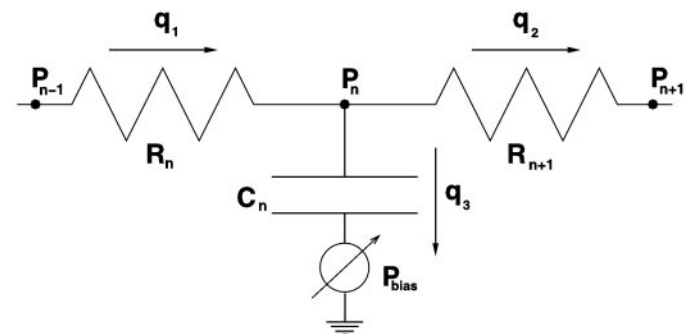


Fig. 1. Single-compartment circuit representation. P, pressure; R, resistance; C, compliance;  $q_1$ ,  $q_2$ , and  $q_3$ , blood flow rates as indicated;  $n - 1$ ,  $n$ ,  $n + 1$ , compartment indexes;  $P_{bias}$ , external pressure.

Applying conservation of mass to the node at  $P_n$  yields  $q_1 = q_2 + q_3$ . Combining these expressions for the flow rates leads to

$$\frac{d}{dt} P_n = \frac{P_{n+1} - P_n}{C_n R_{n+1}} + \frac{P_{n-1} - P_n}{C_n R_n} + \frac{P_{bias} - P_n}{C_n} \cdot \left( \frac{dC_n}{dt} \right) + \frac{d}{dt} P_{bias}$$

The entire model is thus described mathematically by 12 such first-order differential equations. An adaptive step-size fourth-order Runge-Kutta integration routine is used to integrate the system of differential equations numerically. Integration steps range from  $6.1 \times 10^{-4}$  to 0.01 s with a mean step size of  $5.6 \times 10^{-3}$  s. To initiate the numerical integration routine, a set of initial conditions for the state variables (pressures) needs to be supplied. We estimate the initial pressures by a linear algebraic solution of a steady-state version (i.e., all pressures are assumed constant) of the hemodynamic system.

The entire model is shown in Fig. 2. The peripheral circulation is divided into upper body, renal, splanchnic, and lower extremity sections; the intrathoracic superior and inferior vena cavae and extrathoracic vena cava are separately identified. The model thus consists of 12 compartments, each of which is represented by a linear resistance (R) and a capacitance (C) that can be either linear, nonlinear, or time varying.

The pumping action of the heart is realized by varying the right and left ventricular elastances according to a pre-defined function of time [ $E_r(t)$  and  $E_l(t)$ , respectively]

$$E(t) = \begin{cases} E_{dias} + \frac{E_{sys} - E_{dias}}{2} \cdot \left\{ 1 - \cos \left( \pi \cdot \frac{t}{0.3 \sqrt{T(n-1)}} \right) \right\} & 0 \leq t \leq T_S \\ E_{dias} + \frac{E_{sys} - E_{dias}}{2} \cdot \left\{ 1 + \cos \left( 2\pi \cdot \frac{t - 0.3 \sqrt{T(n-1)}}{0.3 \sqrt{T(n-1)}} \right) \right\} & T_S < t \leq \frac{3}{2} T_S \\ E_{dias} & \frac{3}{2} T_S < t \leq T(n) \end{cases}$$

$E_{dias}$  and  $E_{sys}$  represent the end-diastolic and end-systolic elastance values, respectively,  $T(i)$  denotes the cardiac cycle length of the  $i$ th beat, and  $t$  denotes time measured with respect to the onset of ventricular contraction. The systolic time interval,  $T_S$ , is determined by the Bazett formula (2),  $T_S(n) \approx 0.3 \cdot \sqrt{T(n-1)}$ , which links the systolic time interval of the present beat,  $T_S(n)$ , to the duration of the cardiac cycle that preceded it,  $T(n-1)$ .  $T_S$  is determined by the duration of the previous cardiac cycle, but the length of the present cardiac cycle,  $T(n)$ , is determined by means of an integral pulse frequency modulation model of the sinoatrial (SA) node (see, for example, Ref. 36). The efferent (instantaneous) heart rate signal (Eq. 4) is considered a measure of autonomic nervous input to the SA node and is integrated to yield the cumulative input to the SA node over time. A new beat will be initiated once the integral reaches a predefined threshold level as long as the absolute refractory period ( $1.2 \times T_S$ ) has passed since the onset of the previous ventricular contraction.

Figure 3 compares the computed left ventricular elastance (solid line) to experimental data from humans [adapted from Senzaki and co-workers (62)]. The ventricular compliances are computed according to  $C(t) = 1/E(t)$ .

Atria are not represented; their function is, however, partially absorbed into the function of adjacent compartments. Diodes represent valves that ensure unidirectional flow

through the ventricles and parts of the venous system. A time-varying pressure source,  $P_{th}$ , simulates changing transmural pressure across the intrathoracic compartments. We specified the magnitudes of the intrathoracic pressure variations according to Ref. 31, which states that during normal respiration intrathoracic pressure varies between approximately  $-4$  and  $-6$  mmHg. A simple sinusoidal variation between these two values was assumed at a respiratory frequency of 12 breaths/min.

Pressure sources at the abdominal venous compartment ( $P_{bias-3}$ ), the splanchnic ( $P_{bias-2}$ ), and the leg compartment ( $P_{bias-1}$ ) simulate changes in venous transmural pressure due to postural changes or external LBNP.

During high levels of LBNP or during quiet standing, the venous transmural pressures in parts of the dependent vasculature can reach levels at which the nonlinear nature of the venous pressure-volume relationship becomes important (30, 55). In accordance with experimental observations in the legs (46), we model the functional form of the pressure-volume relationships of the venous compartments of the legs, the splanchnic circulation, and the abdominal venous compartment according to Ref. 51

$$\Delta V = \frac{2 \cdot \Delta V}{\pi} \cdot \arctan \left( \frac{\pi \cdot C_0}{2 \cdot \Delta V_{max}} \cdot \Delta P_{trans} \right) \quad (1)$$

where  $\Delta V$  represents the change in compartment volume due to a change in transmural pressure,  $\Delta P_{trans}$ .  $\Delta V_{max}$  is the

maximal change in compartment volume, and  $C_0$  represents the compartment compliance at baseline transmural pressure (i.e., for  $\Delta P_{trans} = 0$ ). Figure 4 shows the pressure volume relationship for the nonlinear venous compliances.

Although the interstitial fluid compartment is not explicitly modeled, total blood volume is modified as a function of time to simulate fluid sequestration into the interstitium during orthostatic stress.

### Parameter Assignments

Where possible, parameter values for the hemodynamic model are based on literature values as indicated in Tables 2 and 3. However, certain values such as the regional systemic resistances had to be estimated.

**Resistances.** On the basis of estimates of the distribution of cardiac output (CO) to the four circulatory branches [upper body (23% of CO), kidney (22% of CO), splanchnic circulation (30% of CO), and lower body (25% of CO)], we modeled arteriolar resistance values to produce a total peripheral resistance of 1.0 peripheral resistance units (PRU = mmHg s/ml). This method generates a splanchnic arteriolar resistance of 3.0 PRU, which is similar to values previously used in cardiovascular models (75). The resistance values on the venous side of the circulation are largely taken from Beneken and DeWitt (3) (see Table 2). Although the pulmonary vascular resistance is known to be nonlinear and dependent on

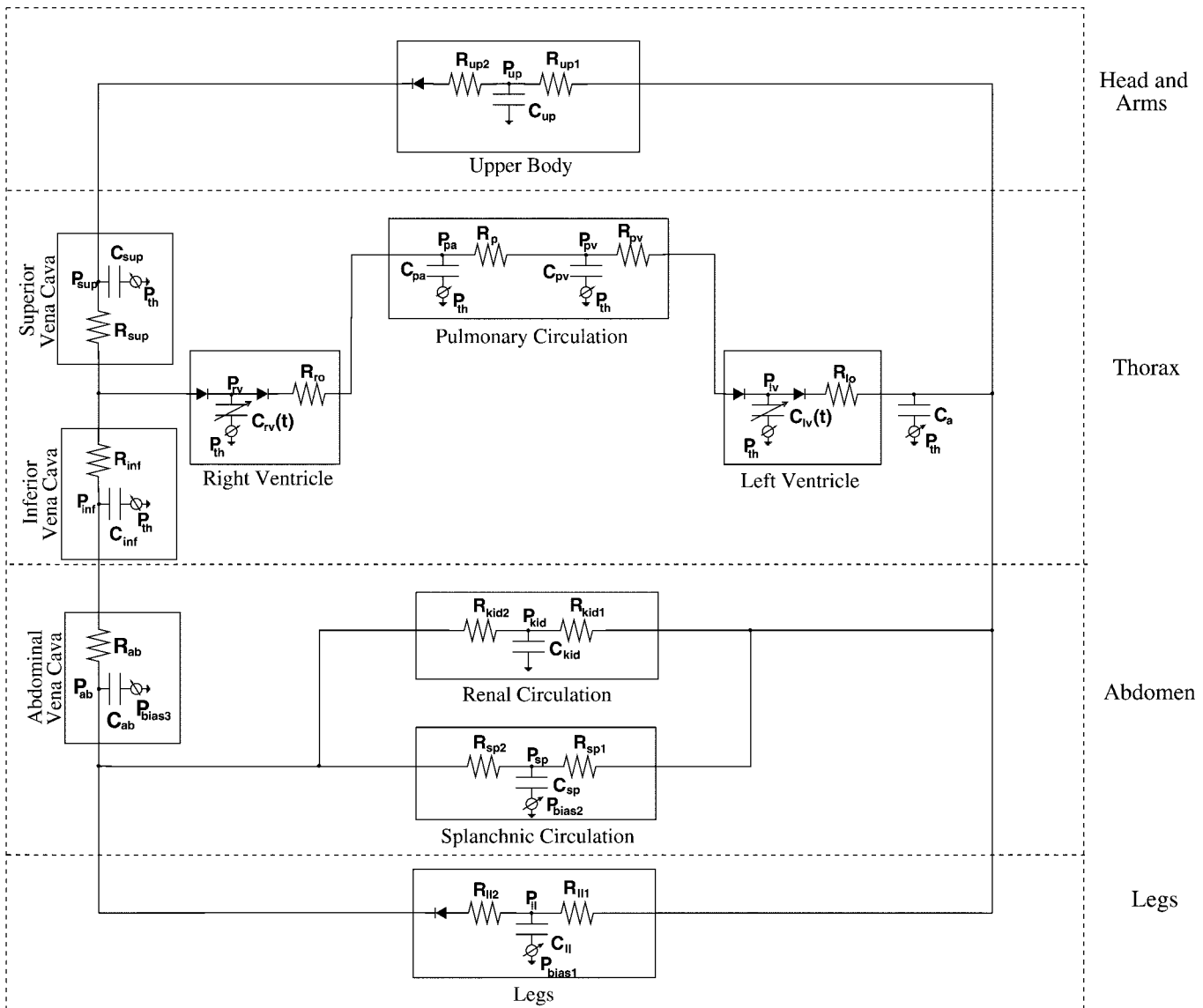


Fig. 2. Circuit diagram of the hemodynamic system. lv, Left ventricle; a, arterial; up, upper body; kid, kidney; sp, splanchnic; ll, lower limbs; ab, abdominal vena cava; inf, inferior vena cava; sup, superior vena cava; rv, right ventricle; p, pulmonary; pa, pulmonary artery; pv, pulmonary vein; ro, right ventricular outflow; lo, left ventricular outflow; th, thoracic; bias, as defined in Fig. 1.

CO, it was approximated by a constant value (52). The outflow resistances of the right and left ventricles ( $R_{ro}$  and  $R_{lo}$ ) have previously been estimated to be 0.003 and 0.01 PRU, respectively (23). The left ventricular inflow resistance is a major determinant of left ventricular filling time during diastole. Consistent with previous estimates (23), we chose the inflow resistance to the left ventricle to be 0.01 PRU, which generates a time constant for ventricular filling of 0.05 s. This value agrees well with observations of filling times of the left ventricle between 0.04 and 0.08 s (13).

**Capacitances.** In addition to being a function of transmural pressure (57), aortic capacitance changes dramatically with age (33). For our purposes, however, it is sufficient to choose the lumped arterial compliance such that the time constant for blood flow from the arterial to the venous side of the systemic circulation found experimentally, 1.9 s, is reproduced (60). This is accomplished by using a lumped arterial compliance of 2.0 ml/mmHg. The venous capacitance value of

the upper body compartment is taken from Beneken and DeWitt (3). The combined capacitance of the splanchnic and kidney compartments is taken to be 70 ml/mmHg with 55 ml/mmHg ascribed to the intestines, liver, and the spleen and 15 ml/mmHg to the kidneys. The leg compartment is assigned a combined venous capacitance of 19 ml/mmHg (34). We modeled the pressure-volume relationships for the abdominal, inferior thoracic, and superior thoracic venae cavae on previous models of the cardiovascular system (19). The lower limb, splanchnic, and abdominal venous compartments all exhibit nonlinear pressure-volume relations according to Eq. 1. The compliances discussed here are the compliances at normal supine transmural pressures ( $C_0$  in Eq. 1). During orthostatic stress, transmural pressures increase in the dependent vascular beds, and the respective compliances are computed by differentiating Eq. 1 with respect to  $\Delta P_{trans}$ . The pulmonary compliances are taken from Beneken and DeWitt (3).

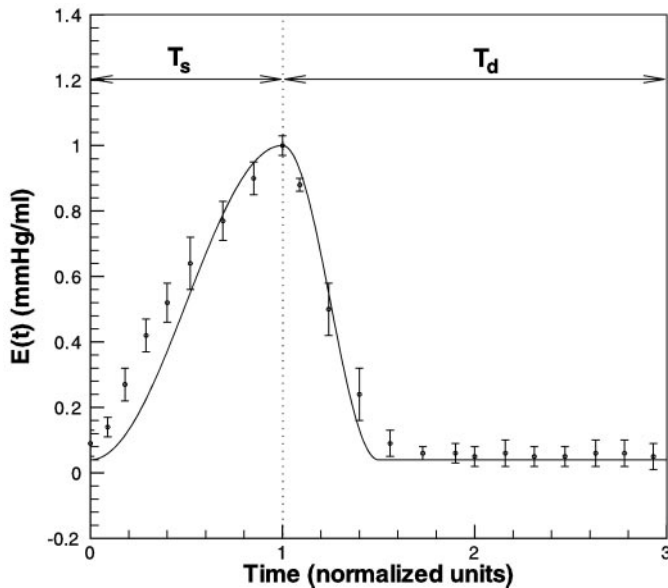


Fig. 3. Time-varying elastance,  $E(t)$ , of the left ventricle during 1 cardiac cycle (solid line) compared with experimental data (●, means  $\pm$  SD; adapted from Ref. 62).  $T_s$ , systolic time interval,  $T_d$ , diastolic time interval.

Both ventricles are characterized by time-dependent compliances that vary between a minimum (end-systolic) and a maximum (diastolic) value according to a predefined functional form (see *Architecture*, above). Previous estimates of maximum diastolic capacitance of 10 ml/mmHg for the left ventricle (20) seem compatible with experimental observations (43). The right ventricular maximum diastolic capacitance ( $C_{diast}^r$ ) is approximately twice the left ventricular value (24). Left ventricular end-systolic capacitance ( $C_{sys}^l$ ) was set to 0.5 mmHg/ml, consistent with recent estimates in humans (62). We choose a value of 1.2 ml/mmHg for right ventricular end-systolic capacitance ( $C_{sys}^r$ ) within the range of experimental values, 0.35 to 1.6 ml/mmHg (24).

**Volume.** Total blood volume is reported to be in the range of 75–80 ml/kg body wt for normal male subjects (28, 66). We set total blood volume to 5,700 ml, corresponding to a 71- to 75-kg normal male subject with a body surface area of 1.7–2.1 m<sup>2</sup>.

Blood volume is reported to be distributed within the circulation approximately as 15% in the aorta, systemic arteries, and arterioles; 69% in the capillaries, venules, and systemic veins; 9% in the pulmonary circulation; and 7% in the heart (31). With an unstressed arterial volume assumed to be 715 ml, the systemic arterial tree contains roughly 900 ml when stressed to a mean arterial pressure of 92 mmHg (715 ml + 2 ml/mmHg  $\times$  92 mmHg), which is  $\sim$ 15% of total blood volume. With the assumption of right and left ventricular filling pressures of 5 and 10 mmHg, respectively, and 50-ml unstressed volumes for each ventricle, the total cardiac volume at end diastole is 300 ml. This is only  $\sim$ 5% of total blood volume, which is partly due to the lack of atria in our

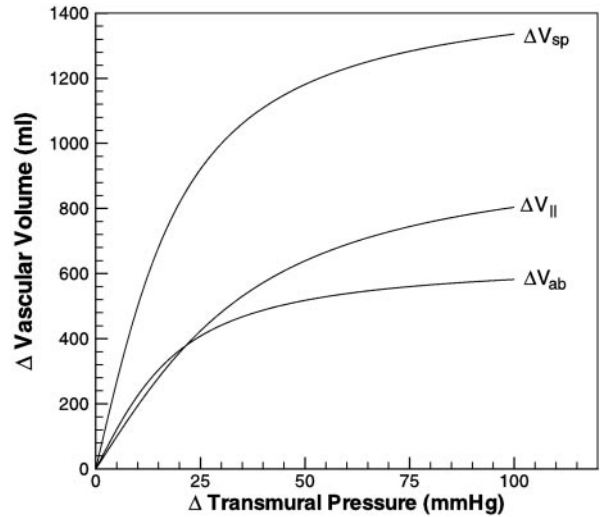


Fig. 4. Pressure-volume relations for changes in stressed volume of the abdominal ( $\Delta V_{ab}$ ), leg ( $\Delta V_{II}$ ), and splanchnic ( $\Delta V_{sp}$ ) venous compartments.

hemodynamic model. Furthermore, there is considerable variation in cardiopulmonary blood volume, ranging from 301 to 546 ml/m<sup>2</sup> of body surface area, as reported by Levinson et al. (45). We adopted Davis' pulmonary unstressed volumes of 90 and 490 ml for the pulmonary arteries and veins, respectively (20). This distribution of arterial and cardiopulmonary blood volumes allocates  $\sim$ 3,600 ml, or 63% of total blood volume, to the capillaries and systemic venous circulation.

Previously published estimates were used for unstressed volumes of the upper body and lower limbs (3), and estimates for the splanchnic venous and central venous compartments were guided by previously published models (75).

The volume and capacitance assignments are summarized in Table 3.

**THE REFLEX MODEL**

*Architecture*

We have adopted and extended a previously reported regulatory set-point model of the arterial baroreflex that aims at maintaining mean arterial blood pressure constant by dynamically adjusting heart rate, peripheral resistance, venous zero-pressure filling volume, and right and left end-systolic cardiac capacitances (20, 22). In addition to this representation of the arterial baroreflex, we have implemented a similar reflex loop to represent the cardiopulmonary reflex, which, at the moment, only affects venous zero-pressure filling volume and systemic arteriolar resistance (see Fig. 5). Briefly, predefined set-point pressures are subtracted from locally sensed blood pressures to generate error functions that are relayed to the autonomic nervous system, where the error signals are rescaled. These error signals subsequently dictate the efferent activity of the reflex model such that the error signals approach zero over the next computational steps.

Table 2. Resistance values

Resistor	R <sub>lo</sub>	R <sub>up1</sub>	R <sub>kid1</sub>	R <sub>sp1</sub>	R <sub>ll1</sub>	R <sub>up2</sub>	R <sub>kid2</sub>	R <sub>sp2</sub>	R <sub>ll2</sub>	R <sub>sup</sub>	R <sub>ab</sub>	R <sub>inf</sub>	R <sub>ro</sub>	R <sub>p</sub>	R <sub>pv</sub>
PRU	0.006	3.9	4.1	3.0	3.6	0.23	0.3	0.18	0.3	0.06	0.01	0.015	0.003	0.08	0.01
Ref.	23	Est.	Est.	Est.	Est.	3	Est.	3	3	3	Est.	3	23	52	23

Est., estimated; PRU, peripheral resistance units. See Figs. 1 and 2 for details.

Table 3. Volume and compliance values

Compartment	ZPFV		Compliance	
	ml	Reference	ml/mmHg	Reference
Right ventricle	50	Estimate	1.2–20	20
Pulmonary arteries	90	21	4.3	3
Pulmonary veins	490	3	8.4	3
Left ventricle	50	Estimate	0.4–10	20
Systemic arteries	715	20	2.0	3
Systemic veins				
Upper body	650	3	8	Estimate
Kidney	150	Estimate	15	Estimate
Splanchnic	1,300	75	55	75
Lower limbs	350	3	19	34
Abdominal veins	250	19	25	19
Inferior vena cava	75	19	2	19
Superior vena cava	10	19	15	19

ZPFV, zero-pressure filling volume.

The input variables to the control system are mean arterial pressure ( $\bar{P}_A$ ) and mean central venous pressure ( $\bar{P}_{CV}$ ) for the arterial baroreflex and the cardiopulmonary reflex as substitutes for carotid sinus ( $\bar{P}_{CS}$ ) and right atrial pressure ( $\bar{P}_{RA}$ ), respectively. The respective error signals are generated by subtracting predefined set-point values ( $\bar{P}_A^{\text{ref}}$  and  $\bar{P}_{CV}^{\text{ref}}$ ) from these input variables and rescaling by an arctangent to generate effective blood pressure deviations ( $P_A^{\text{eff}}$  and  $P_{CV}^{\text{eff}}$ ; Ref. 22)

$$P_A^{\text{eff}} = 18 \cdot \arctan \left( \frac{\bar{P}_A - \bar{P}_A^{\text{ref}}}{18} \right) \quad (2)$$

$$P_{CV}^{\text{eff}} = 5 \cdot \arctan \left( \frac{\bar{P}_{CV} - \bar{P}_{CV}^{\text{ref}}}{5} \right) \quad (3)$$

These mappings are limited to approximately  $\pm 28$  mmHg for the arterial baroreflex and approximately  $\pm 8$  mmHg for the cardiopulmonary reflex and are designed to exhibit the sigmoidicity common to stretch receptors.

To account for differences in timing of the reflex responses, the respective effective blood pressure deviations are weighted by impulse response functions that are characteristic of a parasympathetic  $[p(t)]$  or sympathetic  $[s(t)]$  response (4) (see Fig. 6). The model thus provides for a rapid ( $\sim 0.5 - 1$  s) parasympathetic reflex response and a slower acting ( $\sim 2-30$  s) sympathetic reflex response. A 30-s running history of the effective pressures is used to compute instantaneous effector values by convolution with the appropriate effector specific impulse responses as the following example of R-R interval (I) feedback shows

$$I(t) = I_0 + \int_{k=0}^{k=30} P_A^{\text{eff}}(t-k) \cdot [\beta \cdot p(k) + \gamma \cdot s(k)] dk \quad (4)$$

The contribution of the arterial baroreflex to the instantaneous R-R interval at time  $t$  [ $I(t)$ ] is computed by adding a dynamically computed contribution to the baseline value,  $I_0$ . The impulse response functions,  $p(k)$  and  $s(k)$ , are multiplied by the static gain values,  $\beta$  and  $\gamma$ , for the respective reflex arcs.

During postural changes, hydrostatic pressure at the carotid sinus receptor changes by an amount  $\rho gh \times \sin(\alpha)$ , where  $h$  is the distance of the carotid sinus to the regulated arterial hydrostatic indifference point<sup>1</sup> (27),  $\alpha$  denotes the angle of tilt of the carotid artery measured from the horizon-

tal,  $\rho$  is the density of blood, and  $g$  is the gravitational acceleration. Because our model has only one lumped arterial compartment, we have implemented a bias pressure source ( $\bar{P}_A^{\text{bias}}$ ) which modifies the sensed arterial pressure ( $\bar{P}_A^0$ ) according to

$$\bar{P}_A = \bar{P}_A^0 - \bar{P}_A^{\text{bias}} \quad \text{and} \quad \bar{P}_A^{\text{bias}} = \rho gh \cdot \sin(\alpha) \quad (5)$$

Some experimental evidence exists that the maximum sensitivity of the arterial heart rate baroreflex is linearly related to central venous pressure (54). We implemented this feature by making the R-R interval gain a function of central venous pressure according to

$$\text{Gain}_{\text{R-R interval}} = 1.28 \frac{\text{ms}}{\text{mmHg}} - 0.09 \frac{\text{ms}}{\text{mmHg}^2} \cdot \bar{P}_{CV}$$

#### Parameter Assignments

*Reflex latencies.* Several factors contribute to the time delay between baroreflex stimulation and effector organ response: afferent nerve time response, central nervous processing, efferent transmission, and effector organ response. Borst and Karemaker (9) reported a 0.55-s delay for heart rate response to electrical stimulation of the carotid sinus nerve. They also noted a 2- to 3-s delay for changes in diastolic pressure, which they attributed to reflex changes in peripheral resistance. Berger and co-workers (4) characterized the canine heart rate response to sympathetic and parasympathetic stimulation and reported a reflex latency of  $\sim 1.7$  s for the sympathetic reflex limb. Presently, we use a 0.5-s delay for the parasympathetic reflex response and 2.0 s for all sympathetic reflex arcs.

*Static gain values.* We have adopted DeBoer et al.'s (22) static gain values of 9 ms/mmHg for  $\beta$ -sympathetic feedback and 9 ms/mmHg for parasympathetic feedback, which are based on pharmacological interventions. We incorporated Davis' (20) model of contractility feedback, which states that, under maximal stimulation, the arterial baroreflex can alter end-systolic left and right ventricular cardiac elastances by a factor of 2. In our model, the peripheral resistance and venous tone feedback arcs are influenced by the arterial baroreflex and the cardiopulmonary reflex. Dog experiments revealed a maximum change of systemic reservoir volume of  $\sim 12$  ml/kg under maximal carotid sinus stimulation, 6–7 ml/kg of which have been shown to originate from the abdominal vessels (63). If scaled to represent a 75-kg human, 12 ml/kg maximal deviation in reservoir volume would suggest a maximal zero-pressure volume deviation of 900 ml. Given the limitation of the afferent pressure signal of our arterial baroreflex model to  $\pm 28$  mmHg, 900-ml maximum volume deviation would translate into a static gain value for venous tone feedback of  $\sim 31$  ml/mmHg. Experiments in humans have shown splanchnic blood volume to change by  $\sim 500$  ml in response to a 1,000-ml hemorrhage without significant changes in heart rate, CO, and arteriolar resistance (56). Assuming this response to be mediated by the cardiopulmonary reflex only, we can get a rough estimate of the cardiopulmonary reflex gain to venous tone by assuming that the contribution of the splanchnic circulation is  $\sim 60\%$  of the total venoconstriction response. These assumptions would suggest a static venous tone feedback gain of  $\sim 100$  ml/mmHg because the cardiopulmonary afferent pressure signal is limited to  $\pm 8$  mmHg. The effects of the cardiopulmonary reflex on peripheral resistance can be estimated from LBNP experiments. Low levels of LBNP usually elicit a vasoconstrictor response without increases in heart rate (38, 54). Calculating resistance as (mean arterial pressure – central venous pressure)/

<sup>1</sup>The location of the venous hydrostatic indifference point is discussed in RESULTS.

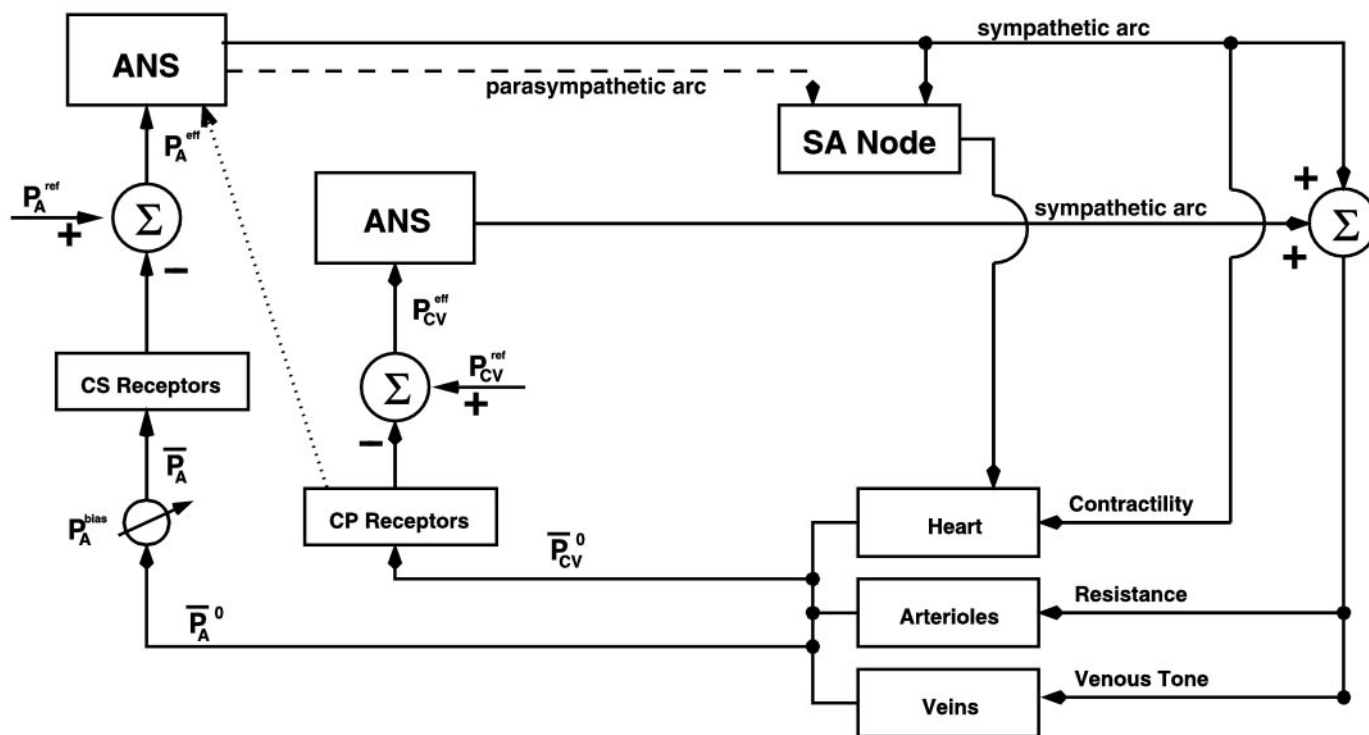


Fig. 5. Diagrammatic representation of the reflex model. CS, carotid sinus; CP, cardiopulmonary; ANS, autonomic nervous system; SA, sinoatrial;  $\Sigma$ , summation. See text for definitions of pressure (P) symbols. The interaction between cardiopulmonary and arterial baroreflex (indicated by dotted line) only affects the maximum sensitivity of the arterial heart rate baroreflex.

CO, the data presented by Pawelczyk and Raven (54) suggest a static gain of the cardiopulmonary arteriolar reflex limb of 0.05–0.06 PRU/mmHg. We followed Davis’s (20) estimate of the peripheral resistance gain of the arterial baroreflex.

Tables 4 and 5 summarize the gain values and the timing of the respective reflex limbs.

**ORTHOSTATIC STRESS TESTS**

Tilt-table and/or stand tests and LBNP interventions are commonly used orthostatic stress tests in both clinical and research environments. Both interventions have in common that increased transmural pressure across the dependent veins provokes a state of central hypovolemia that elicits a sequence of reflex responses.

*Tilt-table Simulation*

A tilt-table intervention leads to rapid blood volume shifts from the thoracic to the dependent vascular beds. Furthermore, the increased transmural pressure in the dependent vasculature leads to increased rates of fluid sequestration into the interstitium and thus a reduction in intravascular volume (32, 37). This second phase of volume redistribution occurs over a much larger timescale than the first one.

To simulate the rapid blood volume shift, the bias pressures across the lower limbs ( $P_{bias-1}$ ), splanchnic ( $P_{bias-2}$ ), and abdominal venous ( $P_{bias-3}$ ) compartments were specified as functions of time

$$P_{bias-i} = \begin{cases} P_{max-i} \cdot \sin [\alpha(t)] & t_0 \leq t \leq t_0 + t_{tilt} \\ P_{max-i} \cdot \sin (\alpha_{max}) & t > t_0 + t_{tilt} \end{cases}$$

where  $\alpha(t)$  represents a ramp function in time from zero to the maximal angle of tilt,  $\alpha_{max}$ . The time to maximal angle is

Table 4. Gain values for the cardiopulmonary reflex

Reflex Limb	Gain Value	Timing	Reference
Peripheral resistance, PRU/mmHg			
Upper body	-0.06	sympathetic	54
Kidney	-0.06	sympathetic	54
Splanchnic	-0.06	sympathetic	54
Lower limbs	-0.06	sympathetic	54
Venous tone, ml/mmHg			
Upper body	13.5	sympathetic	56
Kidney	2.7	sympathetic	56
Splanchnic	54.0	sympathetic	56
Lower limbs	20.0	sympathetic	56

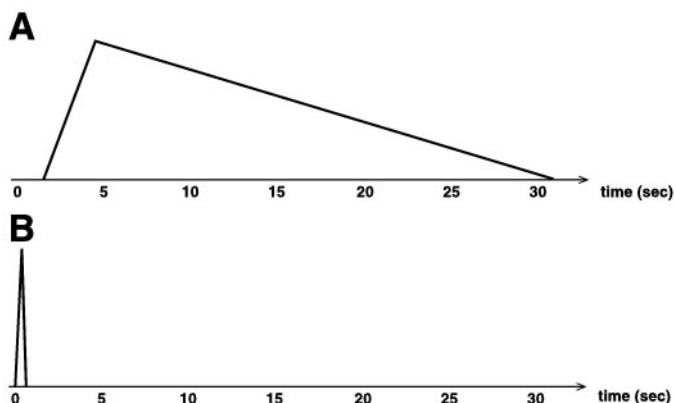


Fig. 6. Sympathetic  $s(t)$ ; A) and parasympathetic  $p(t)$ ; B) impulse response functions.

Table 5. Gain values of the arterial baroreflex

Reflex Limb	Gain Value	Timing	Reference
RR interval, ms/mmHg	9.0	Sympathetic	22
	9.0	Parasympathetic	22
Contractility, ml/mmHg			
LV end-systolic	-0.007	Sympathetic	20
RV end-systolic	-0.021	Sympathetic	20
Peripheral resistance, PRU/mmHg			
Upper body	-0.01	Sympathetic	20
Kidney	-0.01	Sympathetic	20
Splanchnic	-0.01	Sympathetic	20
Lower limbs	-0.01	Sympathetic	20
Venous tone, ml/mmHg			
Upper body	5.3	Sympathetic	63
Kidney	1.3	Sympathetic	63
Splanchnic	13.3	Sympathetic	63
Lower limbs	6.7	Sympathetic	63

LV, left ventricle; RV, right ventricle.

$t_{\text{tilt}}$ , whereas  $t_0$  represents the onset of tilt.  $P_{\text{max-}i}$  denotes the maximal bias pressure across the respective compartment when upright posture is assumed. We chose  $P_{\text{max-}1} = 40.0$  mmHg, which leads to  $\sim 500$  ml of blood being pooled in the leg compartment on assumption of the upright posture (27). We assigned  $P_{\text{max-}2} = 7.0$  mmHg and  $P_{\text{max-}3} = 5.0$  mmHg, which lead to  $\sim 300$  ml of blood being pooled in the abdomen and the pelvis (27).

The slower reduction in blood volume due to fluid loss into the interstitium is modeled by using the work of Hagan and co-workers (32)

$$V_{\text{total}} = (5,700 \text{ ml} - \Delta V) + \Delta V \cdot 0.9 \frac{t-t_0}{60 \text{ s}}$$

The change in blood volume,  $\Delta V$ , has been determined to be  $\sim 600$  ml after 35 min of quiet standing (32). To allow for tilts to different angles, we hypothesized that  $\Delta V$  scales according to

$$\Delta V = 600 \text{ ml} \cdot \sin(\alpha_{\text{max}})$$

#### LBNP Simulation

External negative pressure applied to the lower body is simulated by specifying the bias pressures across the lower body compartment,  $P_{\text{bias-}1} = -P_{\text{LBNP}}$ , according to

$$P_{\text{bias-}i} = \begin{cases} 0 & t < t_0 \\ P_{\text{max}} & t \geq t_0 \end{cases}$$

LBNP is initiated at time  $t_0$ ;  $P_{\text{max}}$  denotes the magnitude of the external negative pressure applied to the lower limbs. In addition to blood pooling in the legs, significant blood pooling occurs in the pelvis and buttocks (77, 81). In our model, the behavior of these two circulatory beds is partly represented by the abdominal venous compartment. Because the latter also represents the great abdominal veins, we simulate blood pooling in the pelvis and buttocks by applying a reduced bias pressure,  $P_{\text{bias-}3} = \epsilon \approx P_{\text{bias-}1}$ , to the abdominal venous compartment ( $\epsilon = 0.3$ ).

The increased hydrostatic pressure gradient across the microcirculation in the lower body and abdominal venous compartments leads to increased rates of fluid sequestration into the interstitium. The total amount of blood volume leaving the vascular system is both a function of level and

duration of LBNP. At high levels of LBNP ( $-70$  to  $-75$  mmHg), it has been shown that a linear net decrease of plasma volume on the order of 500 ml can be observed over the course of 10 min (47). We simulate this plasma volume loss by reducing overall blood volume as a function of LBNP time,  $t - t_0$ , and LBNP level,  $P_{\text{max}}$ , according to

$$V_{\text{total}} = 5,700 \text{ ml} - \Delta V \cdot \frac{t-t_0}{600 \text{ s}} \quad \text{for } 0 \leq t - t_0 \leq 600 \text{ s}$$

where

$$\Delta V = 500 \text{ ml} \cdot \frac{P_{\text{max}}}{70 \text{ mmHg}}$$

#### Matching Experimental Data

When simulating the hemodynamic response of a given subject population, it is usually necessary to adjust the parameters of the model to be able to match a given set of experimental data. In the present study, we chose to compare our simulations to previously published experimental results; thus minimal information about the subject populations was at our disposal. The only variable we were able to match was the peripheral resistance response at different levels of tilt. From the data available, we estimated total peripheral resistance by computing mean arterial pressure/(stroke volume  $\times$  heart rate) for different levels of tilt. We adjusted the static gain values of the peripheral resistance feedback loops to approximate these total peripheral resistance values at the various levels of tilt. After this adjustment, the peripheral resistance gain values were still within physiologically reasonable limits. Subsequently, we used the same parameter settings to simulate the hemodynamic response to LBNP.

#### Testing Hypotheses

Although physiological reasoning can be used to predict qualitatively the impact that a particular parameter might

Table 6. Comparison of steady-state simulation to normal range of hemodynamic parameters

Parameter	Simulation	Normal Range
Cardiac index, $\text{l} \cdot \text{min}^{-1} \cdot \text{m}^{-2}$	3.2	2.8–4.2
Stroke index, $\text{ml} \cdot \text{beat}^{-1} \cdot \text{m}^{-2}$	54	30–65
Pressure, mmHg		
Left ventricle		
Systolic	117	90–140
End-diastolic	9	4–12
Arterial		
Systolic	116	90–140
Diastolic	73	60–90
Venae Cavae		
Maximum	6	2–14
Minimum	4	0–8
Right Ventricle		
Systolic	27	15–28
End-diastolic	2	0–8
Pulmonary artery		
Systolic	27	15–28
Diastolic	13	5–16
Pulmonary artery wedge*		
Maximum	17	9–23
Minimum	11	1–12
Resistance, $\text{mmHg} \cdot \text{ml}^{-1} \cdot \text{s}$		
Total systemic	1.00	0.68–1.05
Total pulmonary	0.12	0.11–0.19

Normal range taken from Ref. 61. \*We approximated pulmonary artery wedge pressure by pulmonary venous and diastolic pressure.

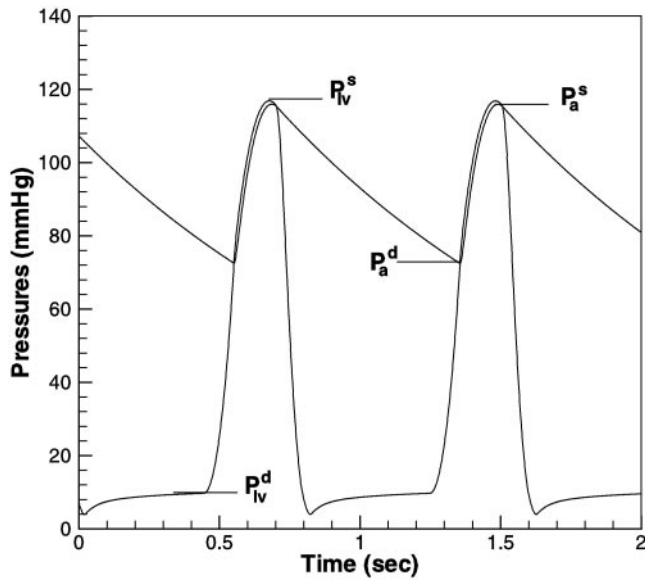


Fig. 7. Simulated central arterial and left ventricular pressure wave-forms.  $P_{IV}^d$ , end-diastolic left ventricular pressure;  $P_{IV}^s$ , systolic left ventricular pressure;  $P_a^d$ , diastolic arterial pressure;  $P_a^s$ , systolic arterial pressure.

have on the hemodynamic response at tilt, the magnitude of the impact can hardly be reasoned. Furthermore, even the qualitative effect of a combination of parameter variations can be difficult to infer. To demonstrate how this model can be used to test hypotheses quantitatively, we focused our attention on the initial heart rate response to tilt. The heart rate response to HUT is usually excessively elevated in patients suffering from OI (53).

We adjusted some of the model parameters (heart rate gain, peripheral resistance gain, and venous tone gain) such that the (baseline) simulated heart rate response to tilt mimics a particular experimental heart rate recording of an astronaut before spaceflight. We subsequently changed four model parameters (blood volume, sympathetic and parasympathetic heart rate gain, combined peripheral resistance gain, and combined venous tone gain) that are assumed to be effected by spaceflight to obtain a sequence of simulations that document the impact that each individual parameter has on the simulated heart rate dynamics. Finally, we compared these simulations as well as a simulation with a combination of effects to the postspaceflight heart rate recording of the same astronaut to see whether any of these simulations match the postflight response.

**RESULTS**

*Baseline Simulation*

Table 6 demonstrates that all major hemodynamic parameters generated by the model are within the range of what is considered physiologically normal in the general population (61).

Representative simulated pressure waveforms are shown in Fig. 7. The figure also demonstrates how

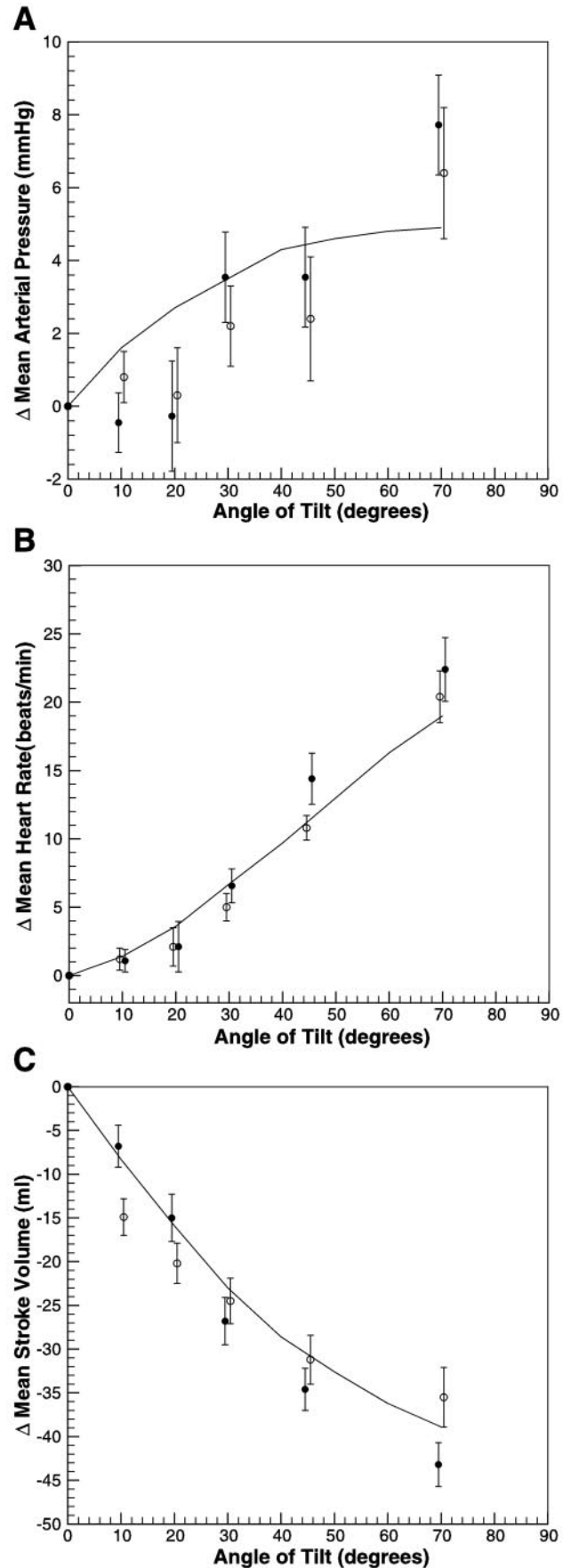


Fig. 8. Comparison of tilt simulations (solid line) to experimental results in 2 age groups (○, men age 40–49; ●, men age 20–29) of mean arterial pressure (A), heart rate (B), and stroke volume (C). Data are means ± SE; adapted from Ref. 67.

systolic and end-diastolic pressures shown in Table 6 were derived from these waveforms.

### Tilt Table Simulation

We simulated the experimental protocol by Smith and co-workers (67), who tilted male subjects to various angles for 5 min with a 5-min supine recovery period between tilts. In accordance with this protocol, we report in Fig. 8 the simulated response (solid line) of mean arterial pressure, heart rate, and stroke volume each averaged over the last 3 min at each level of tilt. Figure 8 also depicts the experimental data recomputed from Ref. 67 to present absolute change and standard error.

Heart rate and stroke volume simulations reproduce the general trend of the experimental data and, within the error bounds of each experiment, match the data at almost every tilt angle. The experimental results of the arterial blood pressure are less conclusive than those reported for heart rate and stroke volume, such that a general trend is hard to discern. The simulation predicts a blood pressure response that is capable of matching the data at most, but not all, levels of tilt.

Figure 9 displays the simulated transient response of heart rate to a rapid HUT (70° over 2 s). It also introduces a number of features of the transient heart rate response measured by Rossberg and Martinez (59) during rapid HUTs (70° over 1.7 s) as a function of respiratory phase in 20 male subjects. Their experimental results are reported in Table 7 along with the feature values extracted from Fig. 9. Although the tilt simulations are not synchronized to the respiratory cycle, the simulated transient response of heart rate generally matches the features reported in Ref. 59

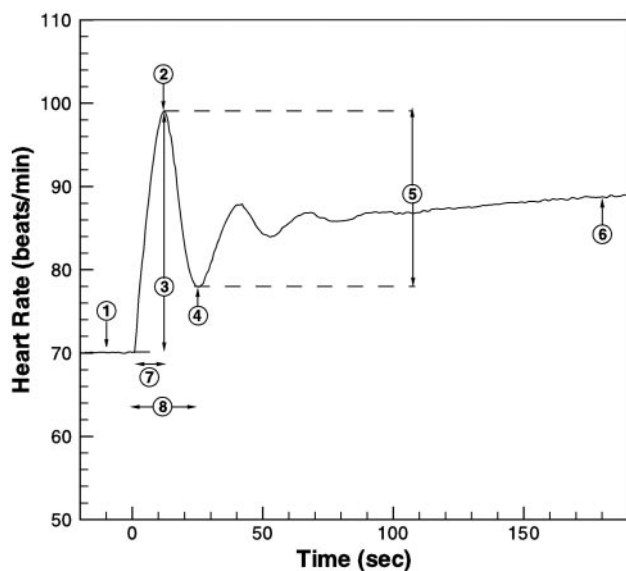


Fig. 9. Features of the simulated heart rate response to a tilt-table experiment (70° head-up tilt over 2 s). 1, Baseline heart rate; 2, peak heart rate; 3, transient increase in heart rate; 4, heart rate trough after peak; 5, drop in heart rate after peak; 6, heart rate at 180 s after initiation of tilt; 7, time to maximal heart rate; 8, duration of initial heart rate transient.

Table 7. Comparison of transient response of heart rate simulation to experimental results

Feature	Unit	Experiment		Simulation
		Expiration	Inspiration	
1	beats/min	59.2 ± 14.6	62.4 ± 7.8	70.1
2	beats/min	92.2 ± 12.1	86.8 ± 10.9	99.1
3	beats/min	29.5 ± 8.4	24.3 ± 6.9	29.0
4	beats/min	75.7 ± 12.9	72.8 ± 10.4	78.0
5	beats/min	17.0 ± 9.5	13.9 ± 6.9	21.1
6	beats/min	89.1 ± 13.1	87.8 ± 13.7	88.7
7	s	7.9 ± 3.9	6.6 ± 3.2	11.7
8	s	15.6 ± 5.0	12.6 ± 4.0	24.9

Values are means ± SD. Expiration, subject is tilted during expiratory phase; inspiration, subject is tilted during inspiratory phase of respiratory cycle. See Fig. 8 and text for definition of features.

within the error bounds of their experiments, the duration of the initial heart rate complex (features 7 and 8) being an exception.

Animal and most human studies agree that the hydrostatic indifference point on the venous side is located at the level of or slightly below the diaphragm (see, e.g., Ref. 27). When a HUT to 90° is simulated, the transmural pressure in the inferior vena cava compartment drops whereas the transmural pressure in the abdominal venous compartment rises, indicating that the venous hydrostatic indifference point in our model is located between these two compartments. This result implies that, as in the human circulation, cardiac filling pressure in our model drops on HUT and therefore cardiac performance is dependent on posture.

### LBNP Simulation

We based simulations of LBNP interventions on the experimental investigation by Ahn and co-workers (1). In accordance with their experimental protocol, we simulated each level of LBNP for 5 min with a sufficient equilibration period (30 min in the experimental study) at normal atmospheric pressures between the various levels. Figure 10 depicts the simulation and experimental results (taken from Ahn and co-workers, Ref. 1) of step changes in LBNP to three levels of negative external pressure. The data and simulations are reported 90 s after the onset of each level of LBNP.

The simulation results of heart rate match the experimental data well whereas the simulation results for mean arterial pressure and stroke volume reproduces the general trend of the data.

### Statistical Analysis

It is our goal to simulate the dynamic response of the cardiovascular system to HUT and LBNP. To test whether our model is capable of representing the experimental data presented in Figures 8 and 10, we used a two-sided test of significance with Bonferroni correction for multiple comparisons. The test indicates that the tilt and LBNP simulations are not statistically different from the 39 data points we presented in Figs. 8 and 10 (15 tilt data points in young subjects; 15 tilt

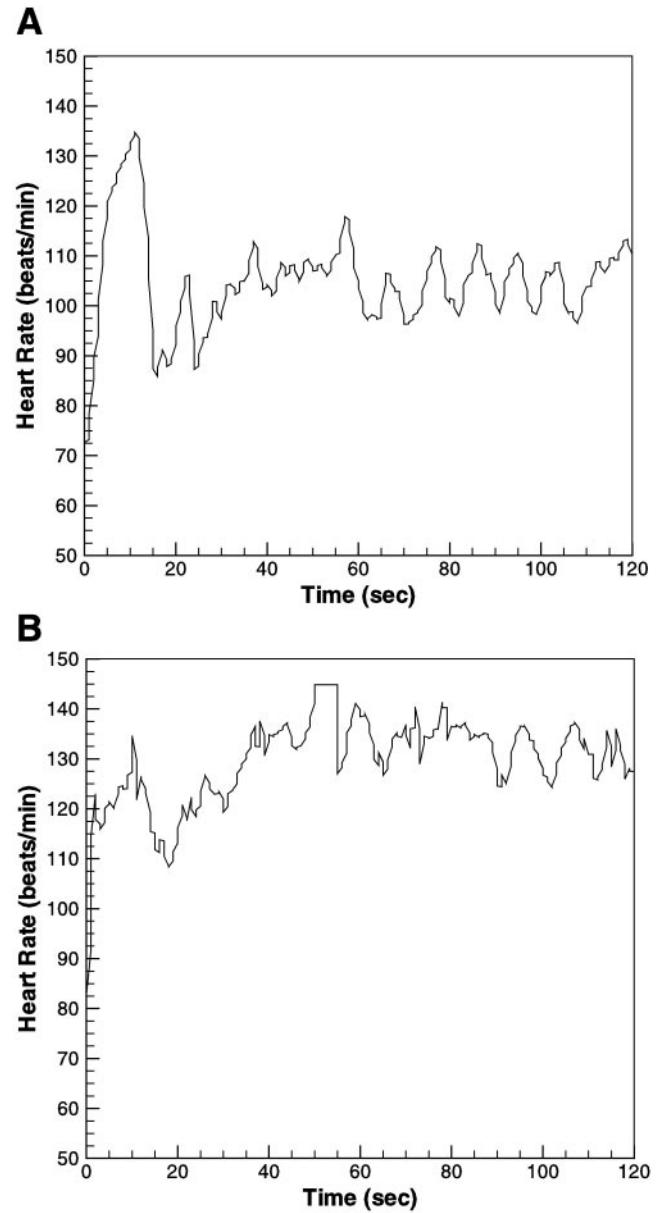
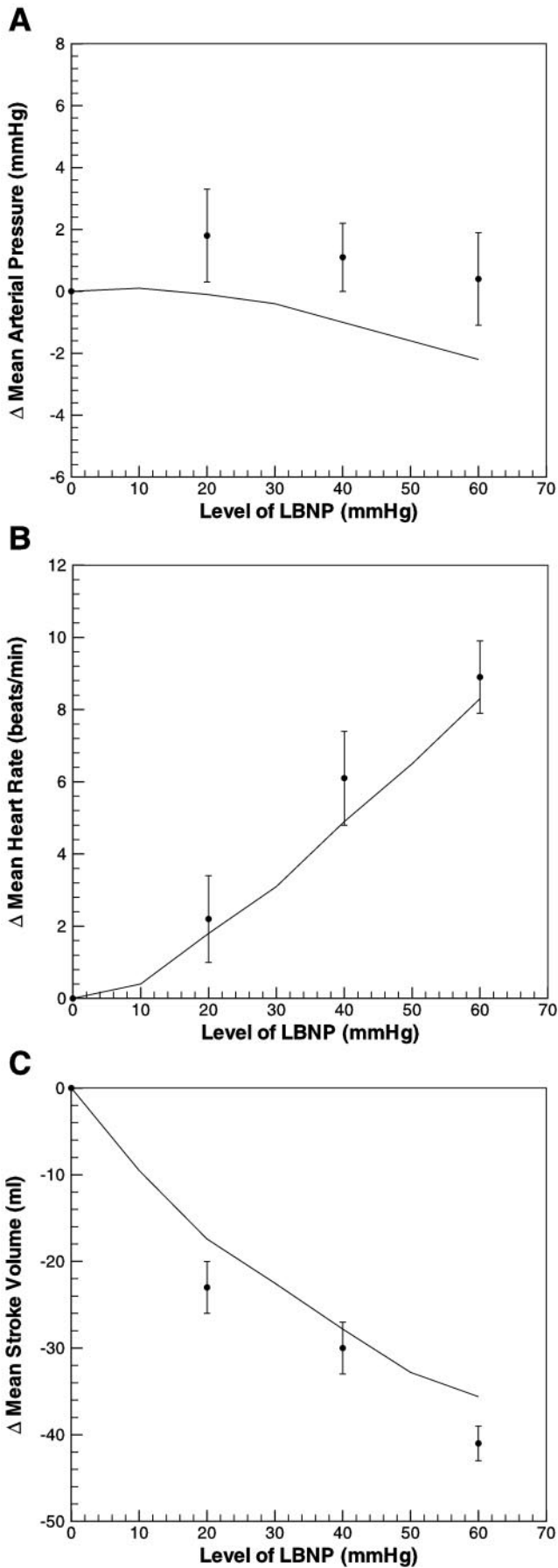


Fig. 11. Heart rate response to standing taken from 1 astronaut 120 days before spaceflight (A) and on landing day (B). Astronaut data provided by Janice Meck, National Aeronautics and Space Administration (NASA), Johnson Space Center, Houston, TX.

data points in older subjects; 9 LBNP data points). The level of significance used is 0.05.

*Testing Hypotheses: An Illustrative Case Study*

The heart rate responses to a stand test of one astronaut 120 days before spaceflight and on landing day are shown in Fig. 11. The postflight heart rate response shows the drastic heart rate increase on assumption of upright posture that is characteristic of

Fig. 10. Comparison of lower body negative pressure (LBNP) simulations (solid line) to experimental results (●) of mean arterial pressure (A), heart rate (B), and stroke volume (C). Data are means ± SE; adapted from Ref. 1.

OI. We simulated the preflight recording by adjusting the combined heart rate gain, combined peripheral resistance gain, and combined venous tone gain, within physiologically reasonable limits. Figure 12 depicts the simulated and actual preflight heart rate responses. Although the match between the two responses is not perfect, the general features and amplitudes are in good agreement. Using the simulated response of Fig. 12 as our baseline, we repeated the simulations for different values of total blood volume (Fig. 13A), combined (parasympathetic and sympathetic) heart rate gain (Fig. 13B), combined peripheral resistance gain (Fig. 13C), and combined venous tone gain (Fig. 13D).

Figure 14 depicts the postspaceflight heart rate recording and a simulated response in which several parameters were changed (blood volume, heart rate gain, venous tone gain, and peripheral resistance gain) to approximate the experimental tracing.

Although total blood volume has the largest impact on the magnitude of the heart rate response, none of the individual simulations is capable of reproducing the dynamics seen in the postflight recording (Fig. 11B).

## DISCUSSION

Mathematical models reflect our present level of understanding of the functional interactions that determine the overall behavior of the system under consideration. They allow us to probe the system, often in much greater detail than is possible in experimental studies, and can therefore help establish the cause of a particular observation.

When fully integrated into an experimental program, mathematical models and experiments are highly synergistic in that the existence of one greatly enhances the value of the other: models, for example,

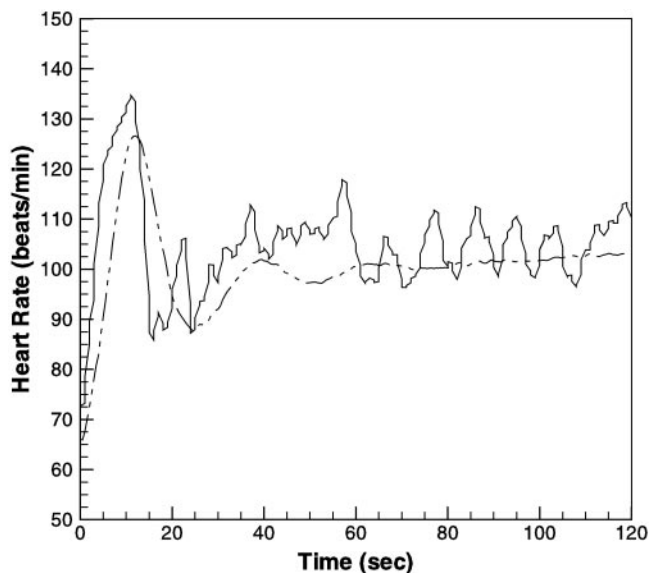


Fig. 12. Simulated (dash-dotted line) and actual heart rate response (solid line) to the upright posture. Experimental data taken 120 days before spaceflight. Astronaut data provided by Janice Meck, NASA, Johnson Space Center, Houston, TX.

depend on experiments for specification and refinement of their parameters, but they also illuminate and enhance the interpretation of experimental results and allow for testing of hypotheses.

The research presented in this paper is part of an ongoing effort to utilize mathematical models in the investigation of the adaptation of the cardiovascular system to a sudden redistribution of blood volume as experienced during a rapid tilt or a LBNP intervention. Our focus rests specifically on the immediate transient and the short-term steady-state response after onset of gravitational stress.

To achieve our objective of simulating the transient and steady-state hemodynamic response to orthostatic stress, we chose to model the entire hemodynamic system by a finite set of representative compartments, each of which captures the physical properties of a segment of the vascular system.

In doing so, we implicitly assume that the dynamics of the system can be simulated by restricting our analysis to relatively few representative points within the cardiovascular system. Although this approach is incapable of simulating pulse wave propagation, for example, it does reproduce realistic values of beat-by-beat hemodynamic parameters (see Table 6). Furthermore, for the same set of parameter values, the simulated steady-state responses to HUT and LBNP agree well with population-averaged experimental observations (see Figs. 8 and 10).

One potential limitation of the hemodynamic system in its present form might be the lack of atria, which are thought to contribute significantly to ventricular filling at high heart rates (6). Although the behavior of stroke volume at high heart rates was not central to the present study, future work might necessitate the addition of atria.

For now, we are restricted to simulating the early steady-state response of the cardiovascular system to orthostatic stress because the reflex control model only represents the major neural control mechanisms that are responsible for short-term ( $\sim 5$  min) control of blood pressure. Studies have shown that within minutes after the onset of gravitational stress, hormone levels in the circulation rise significantly (37). The addition of fast-acting hormone loops in the future will allow us to extend the time scale of our simulations beyond a few minutes.

Our present model does not include the possible dependence of intrathoracic pressure on posture. There is suggestive evidence (48) that intrathoracic pressure decreases on assumption of the upright posture. Such an effect would be expected to modify somewhat the model's response to simulated tilt, and this phenomenon should be investigated more closely in our future studies.

In addition to reproducing steady-state data of hemodynamic variables over a wide range of orthostatic stress levels, the model is capable of reproducing experimentally observed features of the transient heart rate response to rapid tilt (see Table 7 and Fig. 9). Although the amplitudes of the simulated heart rate

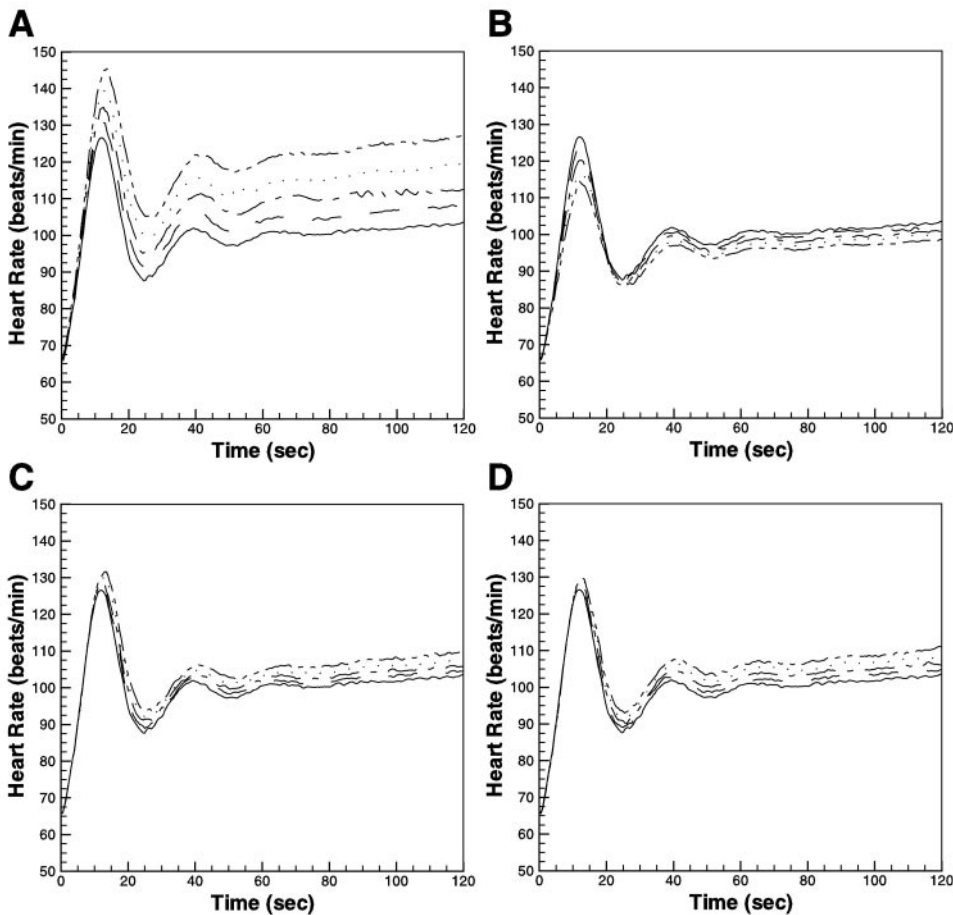


Fig. 13. Simulated heart rate response to rapid tilt to the upright posture ( $90^\circ$ ) for different parameter settings: successive reduction in blood volume (A), heart rate gain (B), venous tone gain (C), and resistance gain (D). Solid line represents baseline simulation. A: tracings are generated by successive removal of blood in 50-ml increments (solid line, total blood volume of 5,700 ml; dashed line, 5,650 ml; dash-dotted line, 5,600 ml; dotted line, 5,550 ml; dash-dot-dotted line, 5,500 ml). B–D: tracings are generated by successive reduction of the respective gain values by 5%.

response match experimental observations well within the variation of the data, the simulations generally predict larger values for the time to maximum heart rate (*feature 7* in Fig. 9) and the duration of the initial

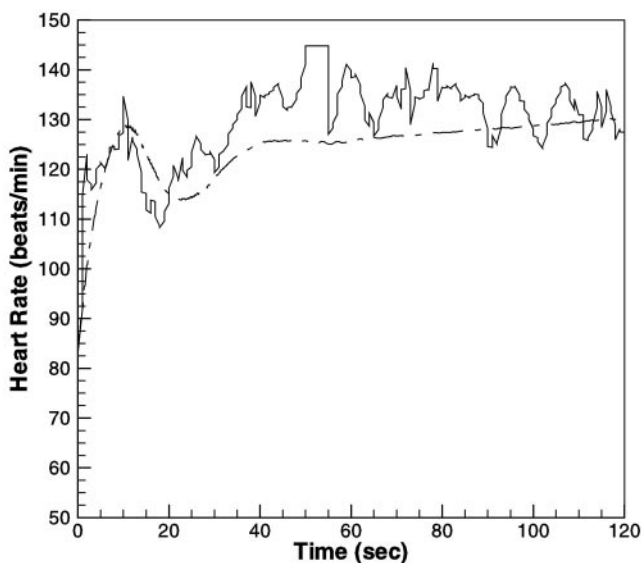


Fig. 14. Simulated (dash-dotted line) and actual heart rate response (solid line) to the upright posture. Experimental data taken on landing day. Astronaut data provided by Janice Meck, PhD, NASA, Johnson Space Center, Houston, TX.

heart rate complex (*feature 8* in Fig. 9). This overestimation can also be seen in Figs. 12 and 14, where we compare our simulations to astronaut data. This fact can be attributed to the sympathetic impulse response function,  $s(t)$  (see Fig. 6): its relatively long duration is primarily responsible for the memory of the reflex system. Truncation of the sympathetic impulse response function will lead to better agreement with the frequency response seen experimentally.

It needs to be pointed out that the transient response of heart rate and blood pressure to rapid tilts has been the focus of many experimental investigations, the results of which seem to fall into two categories: one group of investigations demonstrated a pronounced transient response of heart rate and blood pressure to rapid tilts similar to those seen in standing up (12, 58, 59, 73), whereas a second group of investigations showed a more gradual response to rapid tilts that differ in amplitude and dynamics from the transients encountered during an active change in posture (68–70). Note, however, that the two studies with the largest number of subjects enrolled generally agree on the timing of heart rate increase and subsequent drop (*features 7 and 8* in Fig. 9) whereas the magnitude of the heart rate increase remains controversial (10, 59). We chose to compare our simulation results to the study by Rossberg and Martinez (59) because they provide the most detailed numerical analysis of the

features of the transient heart rate response. So far, we have compared the simulated transient hemodynamic response to tilt to experimental recordings of heart rate only. For future analyses it is desirable to compare the transient simulations to more than one experimental parameter.

An inherent limitation to any modeling effort is the degree of uncertainty with which numerical values can be assigned to the various parameters of the model. We tried as much as possible to give a detailed account of the origin of the parameter values we chose to assign. The degree to which the model reproduces steady-state and transient hemodynamic data suggests that the present model architecture includes all the major features that contribute significantly to the transient and steady-state hemodynamic responses to orthostatic stress.

Figures 12–14 indicate how we intend to use the model to investigate hypotheses regarding the mechanisms underlying postspaceflight OI. Although it is obvious that total blood volume has the strongest effect on the transient heart rate response, none of the parameters, when individually varied, can account for the postflight heart rate dynamics shown in Fig. 11B. It is evident from Fig. 14, however, that if one considers combinations of hypothesized mechanisms, the dynamics of the postflight heart rate response can be reproduced. So far, comparisons between simulations and experiments have relied on visual inspection.

To generate the postflight dynamics from the preflight simulation, we reduced total blood volume by 300 ml, reduced the heart rate gain by 25%, reduced arterial resistance gain by 16%, and reduced venous tone gain by ~5%. Although this result only serves as an example of how we intend to use the model in the future, it is interesting to compare this result to experimental observations obtained from astronauts.

A reduction in blood volume is probably the best documented adaptation to the microgravity environment (see, for example, Ref. 76 for a review of the data). It is commonly thought that a cephalad fluid shift early in microgravity is responsible for a reduction in plasma volume. The magnitude of the observed reduction in blood volume has been reported to range from 342 (25) to 645 ml (39). The reduction in total blood volume necessary in our simulation to approximate the postflight recording is compatible with these experimental findings.

Studies have shown a consistent, yet mostly statistically insignificant, loss of the ability to increase total peripheral resistance (7, 14) and decrease venous diameter (35) postflight. A decreased ability to vasoconstrict has also been documented in animal experiments (5). A working hypothesis of these observations is a possible decrease in peripheral sympathetic neurotransmission: on return to the normal gravitational environment, attenuated vascular responsiveness occurs secondary to end organ hyporesponsiveness (D. Berkovitz and A. A. Shoukas, private communication). The reduction in resistance and venous tone gain val-

ues in the postflight simulation are certainly consistent with the macroscopic effect of this hypothesis.

Finally, we have to introduce a reduction in the combined (sympathetic and parasympathetic) heart rate gain value to approximate the postflight recording. This reduction is consistent with experimental evidence that suggests that the vagal component of the heart rate baroreflex is attenuated after spaceflight (26).

In the manner outlined above, we are confident that the model allows for identification and quantification of the contribution individual parameters have on the transient hemodynamic response to gravitational stress on an individual subject basis.

In summary, we have presented a computational model of the cardiovascular system that has been developed with particular emphasis on the simulation of two common orthostatic stress tests, namely HUT and LBNP. The model generates steady-state and transient hemodynamic responses that compare well to population-averaged and individual subject data. We gave an example of how the model can be used to elucidate the impact that individual parameters have on the transient heart rate response to tilt. By comparing the simulated heart rate response to astronaut data pre- and postspaceflight, we outlined the use of the model as a tool to better understand the changes responsible for postspaceflight OI.

The authors thank Dr. Janice Meck, National Aeronautics and Space Administration (NASA) Johnson Space Center, for kindly providing the astronaut data.

The NASA supported this work through the NASA Cooperative Agreement NCC 9-58 with the National Space Biomedical Research Institute. The first author is grateful for partial support from the Gottlieb Daimler- and Karl Benz-Stiftung.

## REFERENCES

1. **Ahn B, Skakibara Y, Paulev P, Masuda A, Nishibayashi Y, Nakamura W, and Honda Y.** Circulatory and respiratory response to lower body negative pressure in man. *Jpn J Physiol* 39: 919–929, 1989.
2. **Bazett HC.** An analysis of the time-relations of electrocardiograms. *Heart* 7: 353–370, 1920.
3. **Beneken JEW and DeWitt B.** A physical approach to hemodynamic aspects of the human cardiovascular system. In: *Physical Bases of Circulatory Transport: Regulation and Exchange*, edited by Guyton AC and Reeve EB. Philadelphia, PA: Saunders, 1966, p. 1–45.
4. **Berger RD, Saul JP, and Cohen RJ.** Transfer function analysis of autonomic regulation. I. Canine atrial rate response. *Am J Physiol Heart Circ Physiol* 256: H142–H152, 1989.
5. **Berkovitz D, Marucci L, Winters B, Nyhan D, Szumski A, and Shoukas A.** Vascular response in a rate model of microgravity. *Circulation, Suppl* 98: I–128, 1999.
6. **Berne RM, Levy MN, Koeppen BM, and Stanton BA, eds.** *Physiology* (4th ed). St. Louis, MO: Mosby, 1998.
7. **Blomqvist CG, Buckey JC, Gaffney AG, Lane LD, Levine BD, and Watenpaugh DE.** Mechanisms of postflight orthostatic intolerance. *J Gravit Physiol* 1: P-122–P-124, 1994.
8. **Blomqvist LD, Lane CG, Wright SJ, Meny GM, Levine BD, Buckey JC, Peshock RM, Weatherall P, Stray-Gundersen J, Gaffney FA, Watenpaugh DE, Arbeille P, and Baisch F.** Cardiovascular regulation in microgravity. In: *Scientific Results of the German Spacelab Mission D-2: Proceedings of the Norderney Symposium*, edited by Sahm PR, Keller MH, and Schiewe B. Köln, Germany: Wissenschaftliche Projektführung D-2 (c/o Deutsches Zentrum für Luft- und Raumfahrt), 1994, p. 688–690.

9. **Borst C and Karemaker JM.** Time delays in the human baroreflex. *J Auton Nerv Syst* 9: 399–409, 1983.
10. **Borst C, Wieling W, van Brederode JFM, Hond A, de Rijk LG, and Dunning AJ.** Mechanisms of initial heart rate response to postural change. *Am J Physiol Heart Circ Physiol* 243: H676–H681, 1982.
11. **Boyers DG, Cuthbertson JG, and Luetscher JA.** Simulation of the human cardiovascular system: a model with normal response to change in posture, blood loss, transfusion, and autonomic blockade. *Simulation* 18: 197–205, 1972.
12. **Bräuer G and Rossberg F.** Zum Verhalten der Herzfrequenz des Menschen bei unterschiedlichen Geschwindigkeiten der Übergangs vom Liegen zur Kopfaufwärtsbewegung. *Acta Biol Med Ger* 34: 1153–1157, 1975.
13. **Brecher GA and Galletti PM.** Functional anatomy of cardiac pumping. In: *Handbook of Physiology: Circulation*. Bethesda, MD: Am. Physiol. Soc., 1963, sect. 2, vol. II, chapt. 23, p. 759–798.
14. **Buckey JC, Lane LD, Levine BD, Watenpaugh DE, Wright SJ, Moore WE, Gaffney FA, and Blomqvist CG.** Orthostatic intolerance after spaceflight. *J Appl Physiol* 81: 7–18, 1996.
15. **Buckey JC, Lane LD, Plath G, Gaffney FA, Baisch F, and Blomqvist CG.** Effects of head-down tilt for 10 days on the compliance of the leg. *Acta Physiol Scand* 144: 53–60, 1992.
16. **Committee on Space Biology, and Medicine of the National Research Council.** *A Strategy for Research in Space Biology and Medicine for the New Century*. Washington, DC: National Academy Press, 1998.
17. **Convertino VA, Polet JL, Engelke KA, Hoffer GW, Lane LD, and Blomqvist CG.** Evidence for increased  $\beta$ -adrenoreceptor responsiveness induced by 14 days of simulated microgravity in humans. *Am J Physiol Regulatory Integrative Comp Physiol* 273: R93–R99, 1997.
18. **Croston RC and Fitzjerrell DG.** Cardiovascular model for the simulation of exercise, lower body negative pressure, and tilt table experiments. In: *Proc 5th Ann Pittsburgh Conf Modeling Simulation 1974*, 471–476.
19. **Croston RC, Rummel JA, and Kay FJ.** Computer model of cardiovascular control system response to exercise. *J Dyn Syst Meas Contr*, 1973, p. 301–307.
20. **Davis TL.** *Teaching Physiology Through Interactive Simulation of Hemodynamics* (master's thesis). Cambridge, MA: Massachusetts Institute of Technology, 1991.
21. **Davis TL and Mark RG.** Teaching physiology through simulation of hemodynamics. *Comput Cardiol* 17: 649–652, 1990.
22. **DeBoer RW, Karemaker JM, and Stracke J.** Hemodynamic fluctuations and baroreflex sensitivity in human: a beat-to-beat model. *J Appl Physiol* 253: 680–689, 1987.
23. **Defares JG, Osborne JJ, and Hara HH.** Theoretical synthesis of the cardiovascular system. Study I: the controlled system. *Acta Physiol Pharm Neerl* 12: 189–265, 1963.
24. **Dell'Italia LJ and Walsh RA.** Application of a time varying elastance model of right ventricular performance in man. *Cardiovasc Res* 22: 864–874, 1988.
25. **Fischer CL, Johnson PC, and Berry CA.** Red blood cell mass and plasma volume changes in manned space flight. *JAMA* 200: 99–103, 1967.
26. **Fritsch-Yelle JM, Charles JB, Jones MM, Beightol LA, and Eckberg DL.** Spaceflight alters autonomic regulation of arterial pressure in humans. *J Appl Physiol* 77: 1776–1783, 1994.
27. **Gauer OH and Thron HL.** Postural changes in the circulation. In: *Handbook of Physiology: Circulation*. Bethesda, MD: Am. Physiol. Soc., 1965, sect. 2, vol. III, chapt. 67, p. 2409–2439.
28. **Gibson JG and Evans WA.** Clinical studies of the blood volume. II. The relation of plasma and total blood volume to venous pressure, blood velocity rate, physical measurements, age and sex in ninety normal humans. *J Clin Invest* 16: 317–328, 1937.
29. **Goldstein MA, Edwards RJ, and Schroeter JP.** Cardiac morphology after conditions of microgravity during cosmos 2044. *J Appl Physiol* 73, Suppl 2: 94S–100S, 1992.
30. **Griffiths DJ.** Principles of blood flow through collapsible tubes. In: *The Return of Blood to the Heart: Venous Pumps in Health and Disease*, edited by Gardner AMN and Fox RH. London: Libbey, 1993, p. 159–170.
31. **Guyton AC.** *Textbook of Medical Physiology* (9th ed.). Philadelphia, PA: Saunders, 1996.
32. **Hagan RD, Diaz FJ, and Horvath SM.** Plasma volume changes with movement to the upright position. *J Appl Physiol* 45: 414, 1978.
33. **Hallock P and Benson JC.** Studies on the elastic properties of human isolated aorta. *Am J Physiol* 16: 595–602, 1937.
34. **Henry JP, Slaughter OL, and Greiner T.** A medical massage suit for continuous wear. *Angiology* 6: 482–494, 1955.
35. **Herault S, Fomina G, Alferova I, Kotovskaya A, Poliakov V, and Arbeille P.** Cardiac, arterial and venous adaptation to weightlessness during 6-month Mir spaceflights with and without thigh cuffs (bracelets). *Eur J Appl Physiol* 81: 384–390, 2000.
36. **Hyndman BW and Mohn RK.** A model of the cardiac pacemaker and its use in decoding the information content of cardiac intervals. *Automedica* 1: 239–252, 1975.
37. **Jacob G, Ertl AC, Shannon JR, Furlan R, Robertson RM, and Robertson D.** Effect of standing on neurohumoral responses and plasma volume in healthy subjects. *J Appl Physiol* 84: 914–921, 1998.
38. **Johnson JM.** Human splanchnic and forearm vasoconstrictor responses to reductions of right atrial and aortic pressure. *Circ Res* 34: 515–524, 1974.
39. **Johnson PC, Driscoll TB, and LeBlanc AD.** Blood volume changes. In: *Biomedical Results from Skylab*, edited by Johnston RS and Dietlein LF. Washington, DC: National Aeronautics and Space Administration, 1977, chapt. 26, p. 235–241.
40. **Lathers CM and Charles JB.** Orthostatic hypotension in patients, bedrest subjects, and astronauts. *J Clin Pharmacol* 28, Suppl 10: S29–S32, 1994.
41. **Leach CS, Alfrey CP, Suki WN, Leonard JL, Rambaut PC, Inners LD, Smith SM, Lane HW, and Krauhs JM.** Regulation of body fluid compartments during short-term spaceflight. *J Appl Physiol* 81: 105–116, 1996.
42. **Leonard JJ, Leach CS, and Rummel JA.** Computer simulations of postural change, water immersion, and bedrest: an integrative approach for understanding the spaceflight response. *Physiologist* 22: S31–S32, 1979.
43. **Levine BD, Zuckerman JH, and Pawelczyk JA.** Cardiac atrophy after bedrest deconditioning: a nonneuronal mechanism for orthostatic intolerance. *Circulation* 96: 517–525, 1997.
44. **Levine JD, Buckey JC, Fritsch JM, Yancy CW, Watenpaugh DE, Snell PG, Lane LD, Eckberg DL, and Blomqvist CG.** Physical fitness and cardiovascular regulation: mechanisms of orthostatic intolerance. *J Appl Physiol* 70: 112–120, 1991.
45. **Levinson GE, Pacifico AD, and Frank MJ.** Studies of cardiopulmonary blood volume. *Circulation* 33: 347–356, 1966.
46. **Ludbrook J.** Aspects of venous function in the lower limbs. Springfield, IL: Thomas, 1966.
47. **Lundvall J, Bjerkhoel P, Ivarsson C, and Länne T.** Dynamics of transcapillary fluid transfer and plasma volume during lower body negative pressure. *Acta Physiol Scand* 147: 163–172, 1993.
48. **Mead J and Gaensler EA.** Esophageal and pleural pressures in man, upright and supine. *J Appl Physiol* 14: 81–83, 1959.
49. **Melchior FM, Srinivasan RS, and Charles JB.** Mathematical modeling of the human cardiovascular system for simulation of orthostatic response. *Am J Physiol Heart Circ Physiol* 262: H1920–H1933, 1992.
50. **Melchior FM, Srinivasan RS, and Clère JM.** Mathematical modeling of the human response to LBNP. *Physiologist* 35, Suppl 1: S204–S205, 1992.
51. **Melchior FM, Srinivasan RS, Thullier PH, and Clère JM.** Simulation of cardiovascular response to lower body negative pressure from 0 mmHg to –40 mmHg. *J Appl Physiol* 77: 630–640, 1994.
52. **Milnor WR.** Pulmonary hemodynamics. In: *Cardiovascular Fluid Dynamics*, edited by Bergel DH. London: Academic, 1972, p. 299–340.
53. **Narkiewicz K and Somers VK.** Chronic orthostatic intolerance. *Circulation* 98: 2105–2107, 1998.
54. **Pawelczyk JA and Raven PB.** Reductions in central venous pressure improve carotid baroreflex response in conscious men. *Am J Physiol Heart Circ Physiol* 257: H1389–H1395, 1989.

55. **Pollack AA and Wood EH.** Venous pressure in the saphenous vein at the ankle in man during exercise and changes in posture. *J Appl Physiol* 1: 649–662, 1949.
56. **Price HL.** Hemodynamic and metabolic effects of hemorrhage in man with particular reference to the splanchnic circulation. *Circ Res* 18: 469–474, 1966.
57. **Remington JW and Hamilton WF.** The construction of a theoretical cardiac ejection curve from the contour of the aortic pressure pulse. *Am J Physiol* 144: 546–556, 1945.
58. **Rossberg F and Balla K.** Zur Genese des initialen Herzfrequenzverlaufes bei der Kipptischuntersuchung und dessen Wert für die Beurteilung der autonomen Integrität. *Z Gesamte Inn Med* 41: 221–226, 1986.
59. **Rossberg F and Martinez L.** Das Übergangsverhalten der Herzfrequenz des Menschen in Abhängigkeit von der Atemphase während des schnellen, passiven Lagewechsels. *Eur J Appl Physiol* 50: 291–300, 1983.
60. **Sato T.** Parameter sensitivity analysis of a network model of systemic circulatory mechanics. *Ann Biomed Eng* 2: 289–306, 1974.
61. **Schlant RC, Sonnenblick EH, and Katz AM.** Normal physiology of the cardiovascular system. In: *Hurst's The Heart* (9th ed.). New York: McGraw-Hill, 1998, chapt. 3, p. 113–115.
62. **Senzaki H, Chen C, and Kass DA.** Single beat estimation of end-systolic pressure-volume relations in humans. *Circulation* 94: 2497–2506, 1996.
63. **Shoukas AA and Brunner MC.** Epinephrine and the carotid sinus reflex: influence on capacitive and resistive properties of the total systemic vascular bed of the dog. *Circ Res* 47: 249–257, 1980.
64. **Simanonok KE, Srinivasan EE, Myrick RS, Blomkalns AL, and Charles JB.** A comprehensive guyton model analysis of physiologic responses to preadapting the blood volume as a countermeasure to fluid shifts. *J Clin Pharmacol* 34: 440–453, 1994.
65. **Simanonok KE, Srinivasan RS, and Charles JB.** A computer simulation study of preadaptation of the circulation by removal of different blood volumes to counteract fluid shifts. *Physiologist* 35, Suppl 1: S111–S112, 1992.
66. **Sjöstrand T.** Volume and distribution of blood and their significance of regulating the circulation. *Physiol Rev* 33: 202–228, 1953.
67. **Smith JJ, Barney JA, Porth CJ, Groban L, Stadnicka A, and Ebert TJ.** Transient hemodynamic response to circulatory stress in normal male subjects of different ages. *Physiologist* 27: 210, 1984.
68. **Sprangers RLH, Imholz A, Wesseling KH, and Wieling W.** Beat-by-beat analysis of circulatory transients at head-up tilt, bicycle exercise and standing up. *Acta Physiol Scand* 136, Suppl 584: 40, 1989.
69. **Sprangers RLH, van Lieshout JJ, Karamaker JM, Wesseling KH, and Wieling W.** Circulatory response to stand up: discrimination between the effect of respiration, orthostasis and exercise. *Clin Physiol* 11: 221–230, 1991.
70. **Sprangers RLH, Veerman DP, Karamaker JM, and Wieling W.** Initial circulatory response to changes in posture: Influence of the angle and speed of tilt. *Clin Physiol* 11: 211–220, 1991.
71. **Srinivasan RS, and Simanonok JB, and Charles JB.** Computer simulation analysis of the effects of countermeasures for reentry orthostatic intolerance. *Physiologist* 35, Suppl 1: S165–S168, 1992.
72. **Sud VK, Srinivasan R, Charles JB, and Bungo MW.** Effects of lower body negative pressure on blood flow with applications to the human cardiovascular system. *Med Biol Eng Comput* 31: 569–575, 1993.
73. **Sundkvist G and Lilja B.** Effect of degree and speed of tilt on the immediate heart rate reaction. *Clin Physiol* 3: 381–386, 1983.
74. **Tyberg JV and Hamilton DR.** Orthostatic hypotension and the role of changes in venous capacitance. *Med Sci Sports Exerc* 28, Suppl 10: S29–S31, 1996.
75. **Ursino M.** Interaction between carotid baroregulation and the pulsating heart: a mathematical model. *J Appl Physiol* 275: H1733–H1747, 1998.
76. **Watenpaugh DE and Hargens AL.** The cardiovascular system in microgravity. In: *Handbook of Physiology. Environmental Physiology*. Bethesda, MD: Am. Physiol. Soc., 1996, sect. 4, vol. I, chapt. 29, p. 631–674.
77. **White DD and Montgomery LD.** Pelvic blood pooling of men and women during lower body negative pressure. *Aviat Space Environ Med* 67: 555–559, 1996.
78. **White RJ and Blomqvist CG.** Central venous pressure and cardiac function during spaceflight. *J Appl Physiol* 85: 738–746, 1998.
79. **White RJ, Fitzjerrell DG, and Croston RC.** Cardiovascular modelling: simulating the human response to exercise, lower body negative pressure, zero gravity and clinical conditions. In: *Advances in Cardiovascular Physics*. Basel: Karger, 1983, vol. 5, pt. I, p. 195–229.
80. **White RJ, Fitzjerrell DG, and Croston RC.** Fundamentals of lumped compartmental modelling of the cardiovascular system. In: *Advances in Cardiovascular Physics*. Basel: Karger, 1983, vol. 5, pt. I, p. 162–184.
81. **Wolthuis RA, LeBlanc A, Carpentier WA, and Bergman SA.** Response of local vascular volumes to lower body negative pressure stress. *Aviat Space Environ Med* 46: 697–702, 1975.
82. **Yates BJ and Kerman IA.** Postspaceflight orthostatic intolerance: possible relationship to microgravity-induced plasticity in the vestibular system. *Brain Res Brain Res Rev* 28: 73–82, 1998.